Hydrogen-Bonded Pyridine−Water Complexes Studied by Density Functional Theory and Raman Spectroscopy

S. Schlücker,[†] Ranjan K. Singh,[†,§] B. P. Asthana,[‡] J. Popp,[†] and W. Kiefer*[,†]

Institut für Physikalische Chemie, Universität Würzburg, Am Hubland, D-97074 Würzburg, Germany, and Laser and Spectroscopy Laboratory, Department of Physics, Banaras Hindu University, Varanasi 221 005, India

Received: June 12, 2001; In Final Form: August 13, 2001

Density functional theory (DFT) at the B3LYP/6-31++G(d,p) level was employed to obtain the optimized geometries and vibrational spectra of several pyridine(Py)−water(W) complexes with stoichiometric ratios ranging from 2:1 (Py_2W) to 1:3 (PyW_3). The harmonic vibrational wavenumbers of pyridine ring modes and the fundamental modes of water were calculated in order to examine the influence of hydrogen bonding on the normal modes of both pyridine and water upon complexation. The Raman spectra in the wavenumber region 960−1060 cm^{-1} covering the ring modes ν_1 and ν_{12} of pyridine (in Wilson's notation) as a function of pyridine mole fraction were recorded. The integrated Raman intensities in the isotropic components of the spectra were used to determine the relative concentration of "free" pyridine molecules in close neighborhood with other Py−W complexes. The combination of both experimental wavenumbers yielding the overall shift induced by the entirety of hydrogen-bonded complexes in the mixture and the DFT-derived vibrational wavenumbers of the isolated species provides the possibility to probe concentration profiles as a function of pyridine mole fraction. The examination of the concentration dependence of line widths reveals that the counter competing influences of different dynamic processes are simultaneously present in this binary mixture.

1. Introduction

The phenomenon of hydrogen bonding is omnipresent in nature. Hydrogen bonds, for instance, stabilize the secondary and tertiary structures of proteins and are thought to play a major role in molecular recognition, binding, and enzymatic catalysis.[1] Nucleic acid base pairs of polyphosphodiesters, such as of ribonucleic acid (RNA) and deoxyribonucleic acid (DNA), are stabilized by hydrogen bonds between the pyrimidine and purine bases.[2] Quantum chemistry provides concepts to achieve an understanding of the fundamental nature of chemical bonds in general and hydrogen bonds in particular.[3] Structures (optimized geometries), energetics (interaction energies), and vibrational spectra (infrared and Raman) of hydrogen-bonded complexes can be determined via electronic structure calculations. Rigorous ab initio calculations at a very high level can be performed only on small complexes, such as the water dimer, and that too with immense computational effort and cost.[4,5] To predict molecular properties reliably, the inclusion of electron correlation is required. Besides ab initio methods such as Møller−Plesset (MP) theory, density functional theory (DFT) has become very popular recently owing to its good performance (apart from some well-documented problems) and reasonable computational efforts.[6] Binary ionic complexes, complexes of small organic molecules with water, and some other systems have been examined recently.[7−11]

Besides the theoretical methods mentioned above, on the experimental side, the analysis of vibrational line profiles and wavenumber shifts by Raman spectroscopy allows one to study inter- and intramolecular interactions and molecular motions.[12] In contrast to the wavenumber position of a Raman band, which relates to the corresponding force constant(s), basically dependent on electronic structure and bonding, the Raman line width contains information on dynamic aspects (on the time scale of picoseconds/subpicoseconds) in molecular liquids and solids, e.g., on vibrational relaxation (dephasing) and reorientational motions.[13] This was pointed out first in the pioneering work of Gordon.[14] The possibility to separate out these effects by performing polarized Raman measurements, an obvious advantage of Raman spectroscopy over IR spectroscopy, was recognized some years later by Bartoli and Litovitz.[15] The pure isotropic part of the Raman scattered intensity (I_{iso}) provides useful information concerning the vibrational dephasing mechanisms.

Takahashi et al.[16] studied binary mixtures of pyridine with different hydrogen donor solvents including methanol and ethanol spectroscopically. Asthana et al.[17] and Kreyenschmidt et al.[18] made detailed spectroscopic studies on pyridine−methanol mixtures. Vibrational relaxation and chemical exchange broadening in the pyridine−ethanol and pyridine−water systems were examined by Çabaco et al.[19] and Zoidis et al.,[20] respectively. In the work of Deckert et al.[21] on pyridine−ethanol mixtures, structures for the dimer, $C_5H_5N\cdots HOC_2H_5$, and the trimer, $C_5H_5N\cdots(HOC_2H_5)_2$, were calculated on a semiempirical level. Despite the low level of theory, the wavenumber shift of the pyridine ring breathing mode due to hydrogen bonding was adequately explained in a qualitative manner.

The pyridine−water system was chosen for the present study as a model system of a basic N-heterocyclic compound and the most important solvent in biological systems. Dkhissi et al.[22] reported recently a detailed DFT study on the pyridine−water complex employing various local and nonlocal exchange correlation functionals as well as hybrid approaches, but their study was confined to the 1:1 complex. Different basis sets were used by these authors in order to analyze the importance of

* Corresponding author. E-mail: wolfgang.kiefer@mail.uni-wuerzburg.de.
† Universität Würzburg.
‡ Banaras Hindu University.
§ Present address: Department of Physics, Rajendra College, Jai Prakash University, 843102-Chapra, India.

10.1021/jp0122272 CCC: $20.00
Published on Web 10/10/2001

polarization and diffuse functions for the description of structures and spectral properties of hydrogen-bonded systems.[22] In this study, experimental matrix FT-IR data of the 1:1 pyridine−water complex were also compared with second-order Møller−Plesset perturbation theory (MP2) and DFT results.[22] Other closely related studies report on MP2 calculations on 1:1 pyrrole−water and pyridine−water complexes.[23] MP2 and DFT calculations on complexes of water with methyl-substituted pyridines were also published recently.[24]

In view of the earlier theoretical and experimental studies[16−23] and the fact that pyridine−water should act as a model system, it was thought worthwhile to study the structures and spectra of possible hydrogen-bonded pyridine−water complexes, such as Py_2W, PyW, PyW_2, PyW_3, and to explain the observed spectral features in terms of exchange equilibria. In this report, the DFT-derived optimized geometries and vibrational spectra of several pyridine−water complexes are presented and the changes in structures and spectral features within this series are discussed. The simulated Raman spectra of individual complexes in combination with the wavenumber positions of the blue-shifted ring mode of pyridine in the mixture ($\tilde{\nu}_{1'}$ versus $\tilde{\nu}_1$ in neat pyridine) are used to probe concentration profiles. A qualitative analysis of the concentration dependence of the line widths considers dynamical processes taking place in the mixture, e.g., leading to the phenomenon of concentration fluctuations.

2. Methods

A. Experimental Techniques. Pyridine obtained from Fluka was used without further purification. The $I_{\parallel}$ and $I_{\perp}$ components of the Raman scattered intensity were recorded in the region 960−1060 cm^{-1} with mole fractions of pyridine ranging from $x(Py) = 0.02$ to 1.00 in the ($C_5H_5N + H_2O$) mixture. A Spex 1404 double monochromator with 2400 grooves/mm gratings and a liquid N_2-cooled CCD detector (Photometrics) were employed to record the spectra. The 514.5 nm line of an Ar^+-laser delivering ≈100 mW power at the sample was used for excitation. The entrance slit was kept at ≈0.36 cm^{-1} (50 μm slit width). During the entire measurement, the grating position was kept constant and thus a single window spectrum ensures higher precision in peak position. Further, a small slit width also helps in determining the peak position and line widths with better accuracy. The $I_{\parallel}$ and $I_{\perp}$ components of the Raman scattered intensity were measured for each mixture by turning the polarization of the laser beam by 90° using a double Fresnel rhomb and keeping the analyzer position constant in order to avoid errors due to reflectivity of the gratings. The spectra were recorded for around 30 different mixtures with varying molar ratios of pyridine and water [$x(Py) = 0.02-1.00$].

B. Computational Details. The optimized geometries and vibrational wavenumbers, including IR and Raman intensities as well as depolarization ratios, of various hydrogen-bonded complexes were calculated using density functional theory (DFT). The calculations were performed on a vector parallel computer (vclass, Hewlett-Packard) using the GAUSSIAN98 (Rev. A7) suite of programs.[25] The B3LYP functional[26,27] and the 6-31++G(d,p) basis set were employed. It has already been shown that this level of theory is sufficient to reliably predict molecular geometries as well as vibrational spectra of hydrogen-bonded systems.[22] The internal coordinates were generated using the MOLDEN (Vers. 3.4) program.[28]

3. Results and Discussion

A. Density Functional Calculations. The optimized geometries of several pyridine(Py)−water(W) complexes with different stoichiometric ratios: (a) Py_2W (2:1), (b) PyW (1:1), (c) PyW_2 (1:2), and (d) PyW_3 (1:3) are presented in Figure 1. Geometry optimizations were performed without any constraints. In Table 1, some selected inter- and intramolecular structural data for the different species mentioned above, calculated at the B3LYP/6-31++G(d,p) level, are listed. The calculated structural data for the 1:1 complex from the present study are in nice agreement with those obtained by Dkhissi et al.[22] employing the same hybrid functional and basis set. These values are given in square brackets (see Table 1). From Table 1, it can clearly be seen that in the series: $Py_2W \rightarrow PyW \rightarrow PyW_2 \rightarrow PyW_3$, the hydrogen bond $N_a\cdots H_a$ ($N_b\cdots H_b$) between pyridine and water is successively shortened. In the case of PyW, PyW_2, and PyW_3, the strengthening of the hydrogen bond causes an elongation of the covalent O_1-H_a bond in the water molecule. The same effect on the other covalent bond (O_1-H_b) of the same water molecule is much less pronounced. For the Py_2W complex, however, the interatomic distances for the covalent bonds O_1-H_a and O_1-H_b as well as the hydrogen bonds $N_a\cdots H_a$ and $N_b\cdots H_b$ are practically the same. This is quite expected since the two pyridine rings linked with water are symmetrically placed on both sides of the water molecule. These aromatic residues in the Py_2W complex have a nearly perpendicular orientation with a dihedral angle $H_1-N_a-N_b-H_{1'} = -91.6°$, which may probably be caused as a result of diminished repulsive interactions between the π-electon systems of the pyridine rings as well as the oxgygen lone-pairs of the water molecule. The bond lengths O_2-H_c and O_2-H_d of the second water molecule in the PyW_2 complex are quite close to those of the first water molecule, O_1-H_a and O_1-H_b, respectively. The lengths of the two covalent O−H bonds, however, do not match precisely. This is because of the fact that in PyW_2, although both water molecules are hydrogen-bonded, their

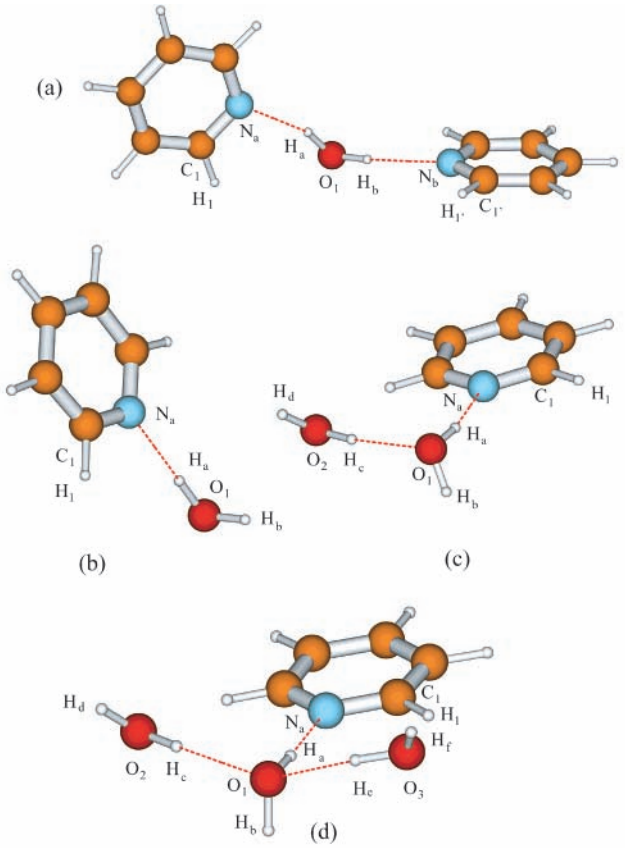

Figure 1. Geometries of pyridine−water complexes optimized at the B3LYP/6-31++G(d,p) level: (a) Py_2W, (b) PyW, (c) PyW_2, (d) PyW_3.

TABLE 1: Some Selected Inter- and Intramolecular Structure Data of Hydrogen-Bonded Pyridine−Water Complexes Calculated at the B3LYP/6-31++G(d,p) Level[a]

bond distances (Å)	Py_2W	PyW	PyW_2	PyW_3
$(N_b\cdots H_b)$	2.0232 (2.0201)	1.9304 [1.93]	1.8236	1.6932
O_1-H_a	0.9747	0.9809 [0.9807]	0.9923	1.0106
O_1-H_b	0.9749	0.9643 [0.9644]	0.9647	0.9663
$O_1\cdots H_c$ $(O_1\cdots H_e)$			1.8300	1.9054 (1.9033)
O_2-H_c (O_3-H_e)			0.9816	0.9778 (0.9779)
O_2-H_d (O_3-H_f)			0.9639	0.9640 (0.9640)
angles (deg)	**Py_2W**	**PyW**	**PyW_2**	**PyW_3**
$H_1-C_1-N_a$ $(H_{1'}-C_{1'}-N_b)$	115.7 (115.7)	116.0	116.2	115.7
$C_1-N_a\cdots H_a$ $(C_{1'}-N_b\cdots H_b)$	105.3 (105.5)	120.1 [122]	127.8	120.4
$N_a\cdots H_a-O_1$ $(N_b\cdots H_b-O_1)$	160.7 (161.2)	177.9 [179]	168.0	175.4
$H_a-O_1-H_b$	106.7	105.8	106.6	106.6
$O_1\cdots H_c-O_2$ $(O_1\cdots H_e-O_3)$			163.6	158.7 (159.0)
$H_c-O_2-H_d$ $(H_e-O_3-H_f)$				106.4 (106.4)

[a] The values for the PyW complex given in square brackets are the ones calculated using the same method and referred from the literature.[22]

TABLE 2: Harmonic Vibrational Wavenumbers (cm^{-1}), Relative Raman Intensities Normalized to the ν_1 and $\nu_{1'}$ Mode, Respectively, Depolarization Ratios of the ν_1, $\nu_{1'}$, and ν_{12} Modes of Pyridine and the Hydrogen-Bonded Pyridine−Water Complexes Calculated at the B3LYP/6-31++G(d,p) Level[a]

	pyridine ring modes			rel. int.	dep. ratio	
species	$\tilde{\nu}_1$	$\tilde{\nu}_{1'}$	$\tilde{\nu}_{12}$	$I_{12}/I_{(1/1')}$	ρ_1	ρ_{12}
Py	1010.1 [1011]		1045.6 [1046]	1.634	0.034	0.032
	989.9 [986]		1024.7 [1020]			
Py_2W		1017.6	1044.9	0.809	0.033	0.033
		997.3	1024.0			
PyW		1020.6 [1021]	1046.1 [1046]	1.106	0.040	0.036
		1000.2 [995]	1025.2 [1020]			
PyW_2		1023.1	1046.5	0.873	0.042	0.043
		1002.6	1025.6			
PyW_3		1028.5	1045.5	0.451	0.042	0.048
		1007.9	1024.6			

[a] The first row and second row show unscaled and scaled values, respectively (scale factor 0.980); values for the PyW complex given in brackets are calculated using the same method referred from literature (scale factor 0.975).[22]

environment is different: the first water molecule being bonded to the N-atom of pyridine (N···H), while the second water molecule is bonded to the O-atom of the first water molecule (O···H). The water−water hydrogen bond ($O_1\cdots H_c$) is slightly longer than the pyridine−water hydrogen bond ($N_a\cdots H_a$). With the addition of a third water molecule yielding the PyW_3 complex, the water−water hydrogen bond ($O_1\cdots H_c$) distance increases. The adjacent covalent bond O_2-H_c is slightly shortened, whereas the effect on the O_2-H_d (O_3-H_f) distance is negligible. This is quite reasonable since these two O−H bonds are open-ended at the H-atom, and are not expected to be appreciably affected by hydrogen bonding. The quite symmetrical structure of the PyW_3 complex is revealed by nearly identical bond distances of the covalent bonds O_2-H_c/O_3-H_e and hydrogen bonds $O_1\cdots H_c/O_1\cdots H_e$, in which both the second and the third water molecule are involved.

The calculated harmonic vibrational wavenumbers of pyridine ring modes (ν_1, $\nu_{1'}$, and ν_{12}), their relative Raman intensities (normalized to ν_1 for neat Py and to $\nu_{1'}$ for all complexes), along with their depolarization ratios in pyridine and the various pyridine−water complexes under consideration are listed in Table 2. All calculated depolarization ratios are extremely small and close to zero as expected for polarized Raman bands. The relative intensities vary in an unexpected and nonsystematic manner. However, not only the Raman scattering activities, but also the normal mode displacement vectors were used for an

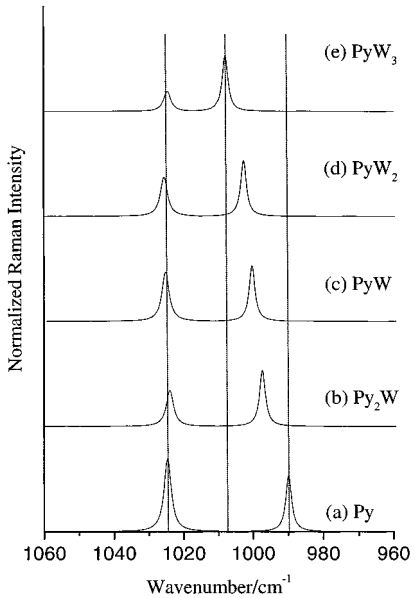

Figure 2. Simulated Raman spectra of pyridine and pyridine−water complexes in the region 960−1060 cm^{-1} along with line width data for $\nu_1/\nu_{1'}$ at ≈990−1008 cm^{-1}: $\Delta\tilde{\nu}_{1/2} = 2.0$ cm^{-1}; and for ν_{12} at ≈1025 cm^{-1}: $\Delta\tilde{\nu}_{1/2} = 2.5$ cm^{-1}.

unambiguous band assignment. Figure 2 displays the simulated Raman spectra of the hydrogen-bonded species in the wavenumber region 960−1060 cm^{-1} based on the data presented in Table 2. It can clearly be seen that in the different complexes, the triangular mode ν_{12} appears at a nearly constant wavenumber position within $\pm < 1$ cm^{-1} as compared to that in neat pyridine. In contrast, the ring breathing mode ν_1 shows a significant shift ($\tilde{\nu}_1 \rightarrow \tilde{\nu}_{1'}$) toward higher wavenumber values with an increasing mole fraction of water in the complexes. The phenomenon of blue-shifting or anti-hydrogen bonds has recently been discussed from a theoretical point of view.[29,30] For the presentation Lorentzian profiles with line widths of 2.0 and 2.5 cm^{-1} for $\nu_1/\nu_{1'}$ and ν_{12}, respectively (see Section 3.B), were assumed. The peak areas were normalized on $\nu_1/\nu_{1'}$, i.e., they present the ratio $I_{12}/I_{(1/1')}$ as listed in Table 2. The theoretical data on the wavenumber position of $\nu_{1'}$ will be used for the comparison with the experimental data in order to check concentration profiles derived from kinetic modeling.[20]

Besides the influence of hydrogen bonding on the electron donor molecule pyridine, also the effects on water as the electron acceptor in this hydrogen-bonded system were studied. The harmonic vibrational wavenumbers of the three normal modes

TABLE 3: Harmonic Vibrational Wavenumbers (cm^{-1}) of the Three Normal Modes of H_2O in Pyridine−Water Complexes Calculated at the B3LYP/6-31++G(d,p) Level[a]

normal mode	Py_2W	PyW	PyW_2	PyW_3[b]
ν_1:				
$\nu_s(H_a-O_1-H_b)$	3618	3538 [3538]	3320	2969
$\nu_s(H_{c,e}-O_{2,3}-H_{d,f})$			3544	3625
ν_2:				
$\delta(H_a-O_1-H_b)$	1652	1637 [1638]	1664	1664
$\delta(H_{c,e}-O_{2,3}-H_{d,f})$			1640	1638 (ip), 1636 (op)
ν_3:				
$\nu_{as}(H_a-O_1-H_b)$	3705	3883 [3881]	3880	3858
$\nu_{as}(H_{c,e}-O_{2,3}-H_{d,f})$			3891	3894 (ip), 3893 (op)

[a] The values for the PyW complex given in square brackets are those calculated using the same method and referred from the literature.[22] [b] (ip): in-phase; (op): out-of-phase.

of H_2O in pyridine−water complexes calculated at the B3LYP/6-31++G(d,p) level are listed in Table 3. The values for the PyW complex given in square brackets are those calculated using the same method and referred from the literature.[22] Within the whole series, the calculated harmonic vibrational wavenumbers resemble with the expected trend on the basis of the O_1-H_a/O_1-H_b bond distances (see Table 1). An elongation of the covalent bond O_1-H_a/O_1-H_b is indicative of a reduced force constant and consequently a lower vibrational wavenumber for the stretching mode. Similar to the preceding discussion of the calculated bond distances, the wavenumber trend of the stretching vibrations ν_1 and ν_3 of water in the series PyW → PyW_2 → PyW_3 and for the Py_2W complex are discussed separately since the latter species has two adjacent aromatic systems (see Figure 1). The deformation mode ν_2 and the asymmetric stretching mode ν_3 of water exhibit only slight shifts, whereas the symmetric stretching mode ν_1 shows significantly large redshifts with an increasing water content in the complex. It should be noted that the use of diffuse function is essential to reliably predict vibrational properties of hydrogen-bonded complexes. Especially the wavenumber value of the ν_1 mode of water is highly sensitive to the inclusion of diffuse functions.[22] For the PyW_3 complex, for instance, ν_1 is predicted to appear below 3000 cm^{-1}, which is even below all aromatic C−H stretching modes (3186−3216 cm^{-1}). The bond distances O_1-H_a and O_1-H_b are miniumum and maximum, respectively, for the Py_2W complex (see Table 1) and show a variation in just-opposite direction in the series: Py_2W → PyW → PyW_2 → PyW_3. The values $\tilde{\nu}_1$ and $\tilde{\nu}_3$ accordingly show the decreasing and increasing trend, respectively, within this series.

Besides the well-known normal modes of pyridine and water, some low-wavenumber modes with considerable IR or Raman activity could be identified in the calculated vibrational spectra. Only the most intense low-wavenumber IR and Raman mode for each complex is listed below. For the IR and Raman active modes the relative intensity I_{rel} given in percent (in parentheses) refers to ν_1 of water ($H_a-O_1-H_b$) and to ν_1 of pyridine, respectively:

$$Py_2W:\ \tilde{\nu}_{IR} = 28\ cm^{-1}\ (5),\ \tilde{\nu}_{Raman} = 27\ cm^{-1}\ (20)$$

$$PyW:\ \tilde{\nu}_{IR} = 104\ cm^{-1}\ (13),\ \tilde{\nu}_{Raman} = 43\ cm^{-1}\ (9)$$

$$PyW_2:\ \tilde{\nu}_{IR} = 174\ cm^{-1}\ (9),\ \tilde{\nu}_{Raman} = 59\ cm^{-1}\ (8)$$

$$PyW_3:\ \tilde{\nu}_{IR} = 159\ cm^{-1}\ (9),\ \tilde{\nu}_{Raman} = 49\ cm^{-1}\ (8)$$

These low wavenumber modes are essentially the librational modes of pyridine and water similar to what one obtains in crystal hydrates. In these modes, there are no intramolecular motions either among the atoms of water or among the atoms of pyridine and the unit (Py or W) as a whole oscillates in the network.

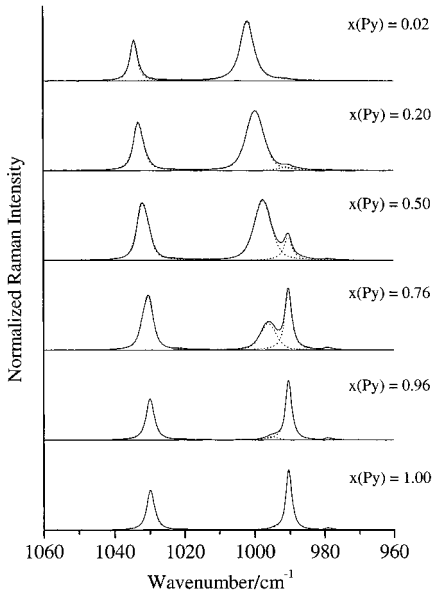

Figure 3. Isotropic components of the Raman spectra of pyridine and pyridine−water mixtures for various mole fractions of water in the region 960−1060 cm^{-1}. The spectra were fitted to three Voigt profiles, except from neat and highly diluted pyridine (x(Py) = 1.00 and 0.02, two Voigt profiles).

B. Spontaneous Raman Spectroscopy. The isotropic components of the linear Raman spectra were determined using a linear combination of $I_{||}$ and $I_{\perp}$ as follows:

$$I_{iso} = I_{||} - 43I_{\perp} \qquad (1)$$

For x(Py) = 1.00 (neat C_5H_5N) and x(Py) = 0.02 (extremely diluted C_5H_5N), the spectra were fitted to two Voigt profiles. The spectra in the concentration range x(Py) = 0.05 to 0.96 were fitted to three Voigt profiles as shown in Figure 3. The bottom spectrum (x(Py) = 1.00) in Figure 3 shows the Raman bands assigned to the ring breathing (ν_1) and the triangular mode (ν_{12}) of neat pyridine (Py) at $\tilde{\nu}_1 \approx 990$ and $\tilde{\nu}_{12} \approx 1030$ cm^{-1}, respectively. The addition of H_2O (W) yields a new broad band at $\tilde{\nu}_{1'} \approx 995-1002$ cm^{-1} in going from pyridine mole fraction x(Py) = 0.96 to 0.02 as shown in Figure 3. This band is obviously due to a network consisting of several distinct hydrogen-bonded species, such as Py_2W, PyW, and PyW_2, as pointed out in the earlier work of Zoidis and co-workers.[20] At mole fraction x(Py) = 0.60 (not shown), nearly the same amount of hydrogen-bonded and "free" pyridine may be assumed to bepresent in view of comparable Raman intensities of the bands at ≈990 and ≈997 cm^{-1}. For very high water concentrations (Figure 3, top spectrum, x(Py) = 0.02), the band associated with the ring breathing mode of "free" pyridine molecules practically vanishes.

In the work of Zoidis et al.,[20] a spectral resolution of 0.6 cm^{-1} was used and the parallel components of the Raman spectra were recorded. The Raman bands at $\tilde{\nu}_1 \approx 990$ cm^{-1}, at $\tilde{\nu}_{1'} \approx 995-1002$ cm^{-1}, and at $\tilde{\nu}_{12} \approx 1030$ cm^{-1} were fitted to one, two, and three profiles, respectively, according to the three species, namely, "free" Py, Py_2W, and PyW_n (including all others), which were included in their model. Although in our Raman spectra presented in Figure 3 a higher spectral resolution (0.36 cm^{-1}) than that of Zoidis et al.[20] was employed for

TABLE 4: Experimental Wavenumber Values (cm^{-1}) of the Pyridine Ring Modes ν_{12}, $\nu_{1'}$ (hydrogen-bonded C_5H_5N), and ν_1 ("free" C_5H_5N) as a Function of Pyridine Mole Fraction

pyridine	wave number			pyridine	wave number		
x(Py)	ν_{12}	$\nu_{1'}$	ν_1	x(Py)	ν_{12}	$\nu_{1'}$	ν_1
1.00	1029.9		990.4	0.50	1031.9	997.6	990.5
0.96	1030.0	995.1	990.4	0.47	1032.0	997.8	990.5
0.92	1030.1	995.3	990.4	0.44	1032.2	998.0	990.5
0.88	1030.3	995.7	990.4	0.43	1032.2	998.0	990.5
0.85	1030.3	995.7	990.4	0.40	1032.3	998.2	990.5
0.82	1030.5	995.9	990.4	0.36	1032.6	998.8	990.6
0.79	1030.5	996.0	990.4	0.33	1032.6	998.8	990.5
0.76	1030.6	996.1	990.4	0.30	1032.8	999.1	990.6
0.74	1030.8	996.4	990.4	0.24	1033.0	999.5	990.7
0.71	1030.9	996.4	990.4	0.20	1033.1	999.7	990.7
0.69	1031.0	996.5	990.4	0.14	1033.4	1000.2	991.3
0.67	1031.1	996.6	990.4	0.10	1033.6	1000.7	993.2
0.63	1031.4	997.0	990.4	0.07	1033.8	1001.0	994.8
0.60	1031.5	997.2	990.5	0.05	1034.0	1001.3	995.4
0.57	1031.6	997.3	990.5	0.02	1034.4	1001.9	
0.53	1031.8	997.5	990.5				

recording the spectra, a distinct shoulder could not be identified to legitimate a fit to more than a single profile. Any attempt to fit, for example, the new band at $\tilde{\nu}_{1'} \approx 995-1002$ cm^{-1} to two profiles proved abortive and led to nearly identical central wavenumber positions of the two peaks at several concentrations. The difference in the spectral features presented in Figure 3 and those obtained by Zoidis et al.[20] are attributed to the fact that at higher water contents the pyridine ring modes under investigation become depolarized. Therefore, the perpendicular component due to the contribution in terms of its intensity, line width, and also central wavenumber position should not be neglected, especially not if minute changes in the Raman spectra are discussed. Furthermore, as discussed above, the DFT calculations yielded distinct wavenumber positions ($\tilde{\nu}_{1'}$) for the PyW, PyW_2, and PyW_3 complexes (see Figure 2 and Table 2) so that condensing all these complexes in "one" PyW_n species and taking this as a model complex[20] seems to be questionable. Thus, the band profile and the wavenumber position of the band at $\tilde{\nu}_{1'} \approx 995-1002$ cm^{-1} as a function of pyridine mole fraction is attributed to a uniform or homogeneous hydrogen-bonded network (i.e., in which isolated species cannot be identified) whose composition (in terms of all possible ratios between pyridine and water) is reflected by the wavenumber position $\tilde{\nu}_{1'}$.

C. Concentration Dependence of Wavenumber Shifts. The wavenumber values of the pyridine ring modes ν_{12}, $\nu_{1'}$, and ν_1 for mole fractions of pyridine ranging from x(Py) = 0.02 to 1.00 are listed in Table 4. Both the triangular mode ν_{12} and the ring breathing mode $\nu_{1'}$ of hydrogen-bonded pyridine molecules show a significant wavenumber shift upon dilution from 1029.9 cm^{-1} at x(Py) = 1.00 to 1034.4 cm^{-1} at x(Py) = 0.02 and 995.1 at x(Py) = 0.96 to 1001.9 cm^{-1} at x(Py) = 0.02, respectively. The ring breathing mode ν_1 of "free" pyridine exhibits only a very small wavenumber shift from 990.4 to 990.7 cm^{-1} within the mole fraction range x(Py) = 1.00 to 0.20 which is quite consistent with earlier results.[21] On increasing the degree of pyridine dilution further, this band also shows a significant wavenumber shift and assumes a value of 995.4 cm^{-1} at x(Py) = 0.05. This indicates that for extreme dilutions [x(Py) ≤ 0.20], almost all pyridine molecules are probably involved in hydrogen bonding. The peak position $\tilde{\nu}_1$ of "free" pyridine approaches the value $\tilde{\nu}_{1'}$ for high pyridine mole fractions.

A comparison with the DFT-derived vibrational spectra presented in Figure 2 reveals that the shift of the ring breathing mode ($\tilde{\nu}_1 \rightarrow \tilde{\nu}_{1'}$) caused by the pyridine−water hydrogen bond

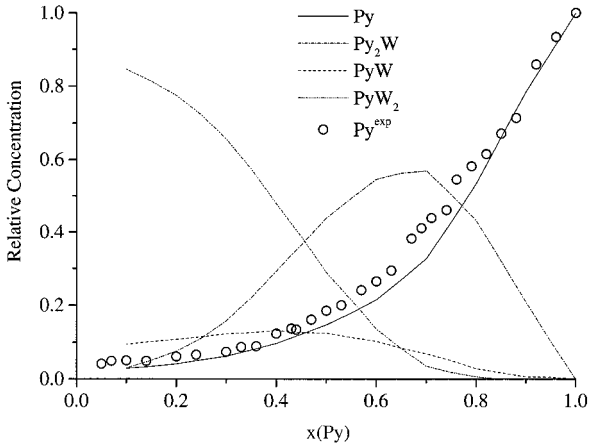

Figure 4. Relative concentration of "free" pyridine (hollow circles) as a function of pyridine mole fraction calculated from the ratio of peak areas, $A_1/(A_1 + A_{1'})$ of integrated Raman intensities A_1 and $A_{1'}$ being the peak areas of the bands at $\tilde{\nu}_1 \approx 990$ cm^{-1} and at $\tilde{\nu}_{1'} \approx 995-1002$ cm^{-1}, respectively, in Figure 3 along with the concentrations of other complexes.

formation matches nicely with what is observed experimentally as shown in Figure 3. In the simulated spectra, however, the systematic wavenumber shift of $\tilde{\nu}_{12}$ is not covered. This may be attributed to the simple model that we have assumed, wherein only isolated species, instead of a whole hydrogen-bonded network, are considered. The latter approach would include distinct hydrogen-bonded species in neighborhood of one another, e.g., Py_2W_3 = PyW + PyW_2, to take care of the environmental effect. A complete simulation of such a whole network is, however, not the central subject of this report.

D. Probing Concentration Profiles. The concentration profile for the pyridine−water system adopted from Zoidis et al.[20] derived through kinetic modeling is presented in Figure 4. In this model, certain chemical equilibria among "free" Py, Py_2W, PyW, and PyW_2 were assumed. One basic assumption in our work is that the band at $\tilde{\nu}_1 \approx 990$ cm^{-1} is associated only with "free" and that the new broad band at $\tilde{\nu}_{1'} \approx 995-1002$ cm^{-1} corresponds to an overall shift $\tilde{\nu}_1 \rightarrow \tilde{\nu}_{1'}$ due to hydrogen-bonded complexes, such as Py_2W, PyW, and PyW_2 being present in a certain ratio in the mixture. From the corresponding integrated Raman intensities, i.e., the peak areas A_1 and $A_{1'}$, the relative concentration of "free" Py to that of complexes was obtained by determining the ratio $A_1/(A_1 + A_{1'})$. This includes the assumption that the Raman scattering cross section of the pyridine ring breathing mode in "free" pyridine and in the hydrogen-bonded species is the same. As shown in Figure 4, the relative concentration of pyridine (hollow circles) obtained from the presented experimental data show only a slight deviation from the profile (solid line) given by Zoidis et al.[20] For a given concentration of "free" Py [x(Py)], the sum of the concentrations of all hydrogen-bonded species present in the mixture can easily be calculated to be [1 − x(Py)]. However, the relative concentrations of the different complexes still remain unknown. A good probe for these concentrations is the wavenumber position $\nu_{1'}$ which lies in the range ≈ 995−1002 cm^{-1}. The basic idea in estimating these concentrations is that the overall shift can be expressed as a linear combination of weighted individual $\tilde{\nu}_{1'}$ values as follows: Since only all the hydrogen-bonded species together contribute to the shifted band at $\tilde{\nu}_{1'} \approx 995-1002$ cm^{-1}, their mole fractions $x(i)$ from Figure 4 were normalized [$x(i) \rightarrow x'(i)$] to the sum of concentrations of hydrogen-bonded species, such that $x'(Py_2W) + x'(PyW) + x'(PyW_2) = 1$. Each of these $x'(i)$ values is multiplied by the

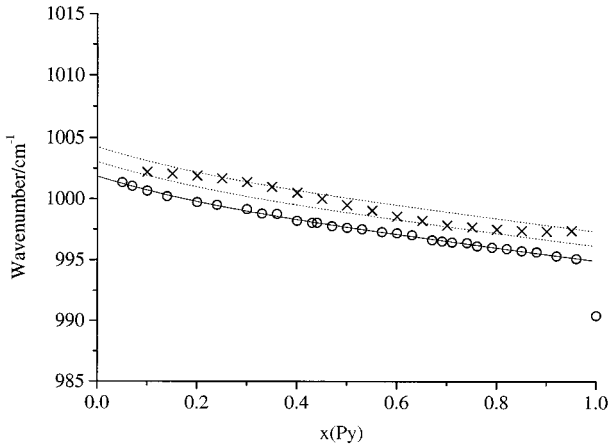

Figure 5. Experimental wavenumber shift of the $\nu_{1'}$ mode of hydrogen-bonded pyridine as a function of pyridine mole fraction (hollow circles), the crosses representing the theoretical values derived from the linear combination [see eq 2 in text], the solid line corresponding to a fourth-order polynomial fit to the experimental values and the two dotted lines vertically shifted by 1.2 and 2.4 cm^{-1}, respectively, representing lower and upper limits of the theoretical values.

corresponding scaled wavenumber $\tilde{\nu}_{1'}$ as reported in Table 2. The overall shift $\tilde{\nu}_{ov}$ can then be expressed as:

$$\tilde{\nu}_{ov}(\text{theo})/\text{cm}^{-1} = [x'(\text{Py}_2\text{W}) \times 997.3 + x'(\text{PyW}) \times 1000.2 + x'(\text{PyW}_2) \times 1002.6]/\text{cm}^{-1} \quad (2)$$

This approach can nicely explain the instantaneous jump of from $\tilde{\nu}_1 \approx 990$ cm^{-1} for "free" Py to $\tilde{\nu}_{1'} \approx 995$ cm^{-1} at $x \geq 0$. By adding the "first droplet" of water, the Py_2W complex is "immediately" formed, yielding $\tilde{\nu}_{1'} \approx 995$ cm^{-1}. The performance of this model can be tested in terms of the observed overestimation of $\tilde{\nu}_{1'} = \tilde{\nu}_{ov}(\text{exp})$ presented in Figure 5. The curve of the experimental values shown in Figure 5 (hollow circles) was fitted to a fourth-order polynomial. The theoretical values (crosses) derived using eq 2 are between the two graphs (dotted lines) which correspond to the same polynomial, but vertically shifted by 1.2 and 2.4 cm^{-1}, respectively. Thus, it is evident that by using this model, the wavenumber positions $\tilde{\nu}_{1'}$ are overestimated in comparison to the experimental values. This, however, arises from an overestimation of the $\tilde{\nu}_1'$ values of the individual hydrogen-bonded species themselves through DFT calculations. A direct comparison of experimental and theoretical values in order to estimate this error is possible only for very low water mole fractions [$x(\text{W}) = 0.04$] since the presence of one single species (Py_2W) can be assumed in this case. The new band appears at $\tilde{\nu}_1' = 995.1$ cm^{-1} for this concentration (see Table 4). From the concentration profile depicted in Figure 4 as well as from "chemical intuition", it can safely be concluded that the Py_2W complex is probably the only hydrogen-bonded species with a significantly high concentration [in terms of its normalized mole fraction $x'(Py_2W)$] as compared with PyW and PyW_2. The scaled harmonic vibrational wavenumber $\tilde{\nu}_1' = 997.3$ cm^{-1} (Table 2) is 2.2 cm^{-1} larger than the experimental value (997.3 cm^{-1}), which lies within the error range depicted in Figure 5.

E. Concentration Dependence of Line Widths. Since this report is aimed primarily at explaining the observed wavenumber shifts in the Raman spectra using DFT-simulated vibrational spectra, the variation of line widths as a function of concentration has been explained only in a qualitative manner. The line width data of the pure isotropic part of the Raman scattered intensity (see Figure 3) for the pyridine ring modes ν_1, $\nu_{1'}$, and

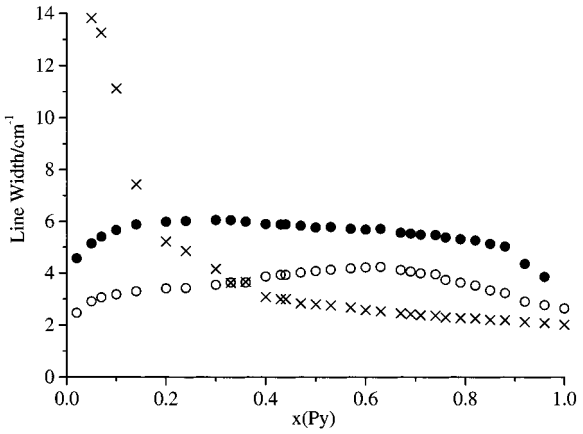

Figure 6. Line width analysis of the ν_1 (crosses), $\nu_{1'}$ (filled circles), and ν_{12} (hollow circles) mode of pyridine as a function of pyridine mole fraction.

TABLE 5: Line Width Data (fwhm in cm^{-1}) for the Ring Modes ν_{12}, $\nu_{1'}$ (hydrogen-bonded C_5H_5N), and ν_1 ("free" C_5H_5N) as a Function of Pyridine Mole Fraction

pyridine	line width $\Delta\tilde{\nu}_{1/2}$			pyridine	line width $\Delta\tilde{\nu}_{1/2}$		
x(Py)	ν_{12}	$\nu_{1'}$	ν_1	x(Py)	ν_{12}	$\nu_{1'}$	ν_1
1.00	2.64		2.01	0.50	4.08	5.77	2.80
0.96	2.77	3.85	2.08	0.47	4.02	5.83	2.84
0.92	2.90	4.36	2.12	0.44	3.93	5.89	3.00
0.88	3.23	5.03	2.19	0.43	3.93	5.88	3.00
0.85	3.33	5.13	2.20	0.40	3.87	5.90	3.09
0.82	3.52	5.26	2.25	0.36	3.64	5.99	3.66
0.79	3.63	5.31	2.28	0.33	3.64	6.05	3.63
0.76	3.74	5.38	2.30	0.30	3.55	6.05	4.17
0.74	3.95	5.47	2.36	0.24	3.42	6.01	4.86
0.71	3.99	5.48	2.38	0.20	3.41	5.98	5.22
0.69	4.06	5.53	2.42	0.14	3.30	5.88	7.43
0.67	4.12	5.56	2.45	0.10	3.18	5.67	11.12
0.63	4.24	5.71	2.53	0.07	3.06	5.41	13.26
0.60	4.22	5.68	2.58	0.05	2.91	5.15	13.82
0.57	4.18	5.71	2.68	0.02	2.47	4.57	
0.53	4.13	5.78	2.76				

ν_{12} as a function of pyridine mole fraction are listed in Table 5. Figure 6 displays the corresponding line width profiles. Similar to other binary mixtures which involve hydrogen bonding, e.g., 3-chloropyridine[31] and chlorobenzene[32] with methanol as a hydrogen-donor solvent, two different kinds of mechanisms causing a line broadening and narrowing are operative, although the broadening mechanism appears to be dominant. For the ring breathing mode ν_1 of "free" Py, a slight increase of $(\Delta\tilde{\nu}_{1/2})_1$ takes place upon dilution up to $x(\text{W}) \approx 0.4$. Below this concentration, a rapid broadening is easily recognized (see Figure 6). A comparison with the concentration profile depicted in Figure 4 reveals that in the latter range, the relative concentration of "free" Py molecules is below 10%. This line broadening at higher dilution is attributed to diffusion, i.e., thesolvent molecules (water) diffusing into the reference system (pyridine). According to the jump diffusion model, a line broadening is caused.[33] It appears that at high dilution, the number of "free" Py molecules is so low that each Py oscillator experiences a collision by all other species present in abundance. This leads to a rapid increase in line broadening below x(Py) ≈ 0.3. The trigonal bending mode ν_{12}, however, exhibits a completely different behavior as compared to ν_1. The presence of a maximum on the $(\Delta\tilde{\nu}_{1/2})_{12}$ vs x(Py) plot is more or less characteristic of dominant concentration fluctuations, which are caused by the random motion of solute (pyridine) molecules throughout the solution volume leading to distinct concentration variations in different micro-volume elements around a mean

value of x(Py) in a Gaussian-like manner. The $(\Delta\tilde{\nu}_{1/2})_{12}$ vs x(Py) plot shows a departure from pure Gaussian behavior, which may be due to the presence of a number of species in complex chemical equilibria. The maximum, however, lies at a x(Py) value close to that where the Py_2W species shows its maximum relative concentration (see Figure 4). It is quite expected since at low dilutions, the hydrogen-bonded complex Py_2W will be present in great abundance. The ring breathing mode $\nu_{1'}$ of hydrogen-bonded pyridine molecules shows more or less a similar trend as reported for ($C_5H_5N + CH_3OH$) mixtures[17] with a difference that a broad plateau between x(Py) $\approx$ 0.3−0.8 is observed instead of a maximum at x(Py) = 0.5. This may probably be attributed to the fact that between x(Py) $\approx$ 0.3−0.8 the different hydrogen-bonded species interchange through complex equilibria leading to a very small change in the line width, although this slight change also shows a steady trend in broadening. In summary, the line width variations in pyridine ring modes in the (Py + W) systems reveal that a complex vibrational dynamics of vibrational modes is operative due to the presence of several species.

4. Conclusions

The optimized geometries and vibrational spectra of neat pyridine and four hydrogen-bonded pyridine−water complexes with different stoichiometric ratios were calculated employing DFT with the hybrid functional B3LYP, using the 6-31++G-(d,p) basis set.

The influence on the vibrational spectra due to hydrogen bonding is monitored by studying in detail the ring breathing mode ν_1 and the trigonal bending mode ν_{12}, of pyridine, and the symmetric O−H stretching mode ν_1 of water. The calculated vibrational spectra of water in different hydrogen-bonded complexes are nicely explained in terms of the influence of hydrogen bonding on bond lengths and force constants of the covalent O−H bonds.

The isotropic components of the Raman spectra show two distinct bands at ≈990 and ≈995−1002 cm^{-1}, which are attributed to "free" pyridine (ν_1) and hydrogen-bonded complexes ($\nu_{1'}$), respectively. A model has been proposed to explain the overall shift of the $\nu_{1'}$ band at ≈995−1002 cm^{-1} measured experimentally as a composite effect of all Py−W complexes in terms of DFT-derived wavenumbers, their relative concentrations based on kinetic modeling in conjunction with intensity ratio $I_1/(I_1 + I_{1'})$. To the best of our knowledge, this is the first study where DFT results have been used to explain the measured Raman shifts and concentration profile in a multicomponent hydrogen-bonded system.

Acknowledgment. S.S. is grateful to the Stipendienfonds im Fonds der Chemischen Industrie and the Bundesministerium für Bildung und Forschung for a postgraduate fellowship. Three of us (S.S., B.P.A., W.K.) acknowledge the support under "DST-DAAD Project Based Personnel Exchange" Program. R.K.S. is thankful to the Alexander von Humboldt-Stiftung for a fellowship. B.P.A. expresses his sincere thanks to the AvH-Stiftung for supporting his visits to the University of Würzburg to maintain an active collaboration. J.P. gratefully acknowledges support from the Freistaat Bayern (Bayerisches Habilitationsförderpreis). W.K. thanks the German Science Foundation and the Fonds der Chemischen Industrie for financial support.

References and Notes

(1) Kirby, A. J. *Acc. Chem. Res.* **1997**, *30*, 290.
(2) Hobza, P.; Šponer, J. *Chem. Rev.* **1999**, *99*, 3247.
(3) Gordon, M. S.; Jensen, J. H. *Acc. Chem. Res.* **1996**, *29*, 536.
(4) Schütz, M.; Brdarski, S.; Widmark, P.-O.; Lindh, R.; Karlström, G. *J. Chem. Phys.* **1997**, *107*, 4597.
(5) van Duijneveldt-van de Rijdt, J. G. C. M.; van Duijneveldt, F. B. *J. Chem. Phys.* **1999**, *111*, 3812.
(6) Koch, W.; Holthausen, M. C. *A Chemist's Guide to Density Functional Theory*; Wiley-VCH: Weinheim, 2000.
(7) Remer, L. C.; Jensen, J. H. *J. Phys. Chem. A* **2000**, *104*, 9266.
(8) Pudzianowski, A. T. *J. Phys. Chem.* **1996**, *100*, 4781.
(9) Rablen, P. R.; Lockman, J. W.; Jorgensen, W. L. *J. Phys. Chem. A* **1998**, *102*, 3782.
(10) Tuma, C.; Boese, A. D.; Handy, N. C. *Phys. Chem. Chem. Phys.* **1999**, *1*, 3939.
(11) Simon, S.; Bertran, J.; Sodupe, M. *J. Phys. Chem. A* **2001**, *105*, 4359.
(12) Asthana, B. P.; Kiefer, W. In *Vibrational Spectra and Structure*; Durig, J. R., Ed.; Elsevier: Amsterdam, 1992; Vol. 20, p 67.
(13) Rothschild, W. G. *Dynamics of Molecular Liquids*; Wiley: New York, 1983.
(14) Gordon, R. G. *J. Chem. Phys.* **1965**, *43*, 1307.
(15) Bartoli, F. J.; Litovitz, T. A. *J. Chem. Phys.* **1972**, *56*, 404, 413.
(16) Takahashi, H.; Mamola, K.; Plyler, E. K. *J. Mol. Spectrosc.* **1966**, *21*, 217.
(17) Asthana, B. P.; Takahashi, H.; Kiefer, W. *Chem. Phys. Lett.* **1983**, *94*, 41.
(18) Kreyenschmidt, M.; Eysel, H. H.; Asthana, B. P. *J. Raman Spectrosc.* **1993**, *24*, 645.
(19) Cabaço, M. I.; Besnard, M.; Yarwood, J. *Mol. Phys.* **1992**, *50*, 139, 157.
(20) Zoidis, E.; Yarwood, J.; Danten, Y.; Besnard, M. *Mol. Phys.* **1995**, *85*, 373, 385.
(21) Deckert, V.; Asthana, B. P.; Mishra, P. C.; Kiefer, W. *J. Raman Spectrosc.* **1996**, *27*, 907.
(22) Dkhissi, A.; Adamowicz, L.; Maes, G. *J. Phys. Chem. A* **2000**, *104*, 2112.
(23) Martoprawiro, M. A.; Bacskay, G. B. *Mol. Phys.* **1995**, *85*, 573.
(24) Pápai, I.; Janscó, G. *J. Phys. Chem. A* **2000**, *104*, 2132.
(25) Frisch, M. J.; Trucks, G. W.; Schlegel, H. B.; Scuseria, G. E.; Robb, M. A.; Cheeseman, J. R.; Zakrzewski, V. G.; Montgomery, J. A., Jr.; Stratmann, R. E.; Burant, J. C.; Dapprich, S.; Millam, J. M.; Daniels, A. D.; Kudin, K. N.; Strain, M. C.; Farkas, O.; Tomasi, J.; Barone, V.; Cossi, M.; Cammi, R.; Mennucci, B.; Pomelli, C.; Adamo, C.; Clifford, S.; Ochterski, J.; Petersson, G. A.; Ayala, P. Y.; Cui, Q.; Morokuma, K.; Malick, D. K.; Rabuck, A. D.; Raghavachari, K.; Foresman, J. B.; Cioslowski, J.; Ortiz, J. V.; Stefanov, B. B.; Liu, G.; Liashenko, A.; Piskorz, P.; Komaromi, I.; Gomperts, R.; Martin, R. L.; Fox, D. J.; Keith, T.; Al-Laham, M. A.; Peng, C. Y.; Nanayakkara, A.; Gonzalez, C.; Challacombe, M.; Gill, P. M. W.; Johnson, B. G.; Chen, W.; Wong, M. W.; Andres, J. L.; Head-Gordon, M.; Replogle, E. S.; Pople, J. A. *Gaussian 98*, revision A.7; Gaussian, Inc.: Pittsburgh, PA, 1998.
(26) Becke, A. D. *J. Chem. Phys.* **1993**, *98*, 5648.
(27) Lee, C.; Yang, W.; Parr, R. G. *Phys. Rev. B* **1988**, *37*, 785.
(28) Schaftenaar, G. *MOLDEN*, 1991.
(29) Cubero, E.; Orozco, M.; Hobza, P.; Luque, F. J. *J. Phys. Chem. A* **1999**, *103*, 6394.
(30) Hobza, P.; Havlas, Z. *Chem. Rev.* **2000**, *100*, 4253.
(31) Singh, R. K.; Asthana, B. P.; Verma, A. L.; Pathak, C. M. *Chem. Phys. Lett.* **1997**, *278*, 35.
(32) Singh, R. K.; Bhriguvansh, P.; Asthana, B. P.; Verma, A. L. *Chem. Phys. Lett.* **1998**, *296*, 611.
(33) Egelstaff, P. A. *An Introduction to Liquid State*; Academic Press: New York, 1967; Chapter 10.